



1 **Pathway dependence of ecosystem responses in China to 1.5°C global warming**

2

3 Xu Yue¹, Hong Liao¹, Huijun Wang², Tianyi Zhang³, Nadine Unger⁴, Stephen Sitch⁴,
4 Zhaozhong Feng¹ and Jia Yang⁵

5

6

7 ¹ Jiangsu Key Laboratory of Atmospheric Environment Monitoring and Pollution Control,
8 Collaborative Innovation Center of Atmospheric Environment and Equipment Technology, School
9 of Environmental Science and Engineering, Nanjing University of Information Science &
10 Technology (NUIST), Nanjing, 210044, China

11 ² Ministry of Education Key Laboratory of Meteorological Disaster, Joint International Research
12 Laboratory of Climate and Environment Change, Collaborative Innovation Center on Forecast and
13 Evaluation of Meteorological Disasters, NUIST, Nanjing, 210044, China

14 ³ State Key Laboratory of Atmospheric Boundary Layer Physics and Atmospheric Chemistry,
15 Institute of Atmospheric Physics, Chinese Academy of Sciences, Beijing, 100029, China

16 ⁴ College of Engineering, Mathematics and Physical Sciences, University of Exeter, Exeter, EX4
17 4QE, UK

18 ⁵ Department of Forestry, Mississippi State University, Mississippi State, MS, 39762, US

19

20 Email: yuexu@nuist.edu.cn and hongliao@nuist.edu.cn

21

22

23

24

25



26

27

28

Abstract

29

30 China is currently the world's largest emitter of both CO₂ and short-lived air pollutants.

31 The ecosystems in China help mitigate a part of its carbon emissions, but are subject to

32 perturbations in CO₂, climate, and air pollution. Here, we use a dynamic vegetation

33 model and data from three model inter-comparison projects to examine ecosystem

34 responses in China under different emission pathways towards the 1.5°C warming

35 target set by the Paris Agreement. At 1.5°C warming, gross primary productivity (GPP)

36 increases by 15.5±5.4 % in a stabilized pathway and 11.9±4.4 % in a transient pathway.

37 CO₂ fertilization is the dominant driver of GPP enhancement and climate change is the

38 main source of uncertainties. However, differences in ozone and aerosols explain the

39 GPP differences between pathways at 1.5°C warming. Although the land carbon sink is

40 weakened by 17.4±19.6 % in the stabilized pathway, the ecosystems mitigate 10.6±1.4%

41 of national emissions in the stabilized pathway, more efficient than the fraction of

42 6.3±0.8% in the transient pathway. To achieve the 1.5°C warming target, our analysis

43 suggests a higher allowable carbon budget for China under a stabilized pathway with

44 reduced emissions in both CO₂ and air pollution.

45

46 **Keywords:** Ecosystems, climate change, 1.5°C warming, emission pathway, ozone

47 vegetation damage

48

49



50 **1 Introduction**

51 The past decade has seen record-breaking warming largely related to anthropogenic
52 greenhouse gas emissions (Mann et al., 2017). This warming trend presents a challenge
53 to achieve the temperature control target of 1.5°C above the pre-industrial (PI) level set
54 by the 2015 Paris climate agreement. Many studies have shown that a conservative
55 warming such as 1.5°C is necessary to limit climatic extremes (Nangombe et al., 2018),
56 avoid heat-related mortality (Mitchell et al., 2018), reduce economic loss (Burke et al.,
57 2018), and alleviate ecosystem risks (Warszawski et al., 2013) compared to stronger
58 anthropogenic warming. To achieve this target, each country must aim to control its
59 greenhouse gas emissions. A full understanding of regional ecosystem response to the
60 changing climate and environmental stress is essential to reduce uncertainties in
61 allowable carbon budget estimates at 1.5°C (Mengis et al., 2018). China is covered with
62 a wide range of terrestrial biomes (Fang et al., 2012). While China's ecosystem
63 response to possible future climate has been explored (Wu et al., 2009; Dai et al.,
64 2016; He et al., 2017), impacts on the regional carbon budget in differing pathways to
65 the 1.5°C target are not known.

66

67 There are two distinct pathways to the 1.5°C global warming. One is a fast process in
68 which global temperature passes 1.5°C and continues to increase (scenarios assuming
69 high CO₂ emissions and no climate mitigation) while the other is a stabilized process
70 with an equilibrium warming right below 1.5°C and last for decades before the end of
71 21st century (scenarios including climate mitigation). The stabilized pathway is the one
72 proposed by the 2015 Paris agreement. However, the unprecedented warming in 2016
73 results in an increase of global average temperature by 1.1°C above PI
74 (<https://public.wmo.int>), suggesting that the 1.5°C limit can be broken in a near future
75 under a transient pathway. A few studies have compared allowable carbon budgets
76 between these two pathways (Millar et al., 2017; Collins et al., 2018), but none has
77 estimated the mitigation potential of regional ecosystems with joint impacts of changes
78 in climate, CO₂, and air pollution under different pathways.

79



80 Here, we apply the Yale Interactive terrestrial Biosphere Model (YIBs) (Yue and Unger,
81 2015; Yue and Unger, 2018) to investigate the response of terrestrial ecosystem
82 productivity in China to both stabilized and transient global warming of 1.5°C relative
83 to PI period. The YIBs model is driven with meteorology from an ensemble of climate
84 models in Climate Model Intercomparison Project Phase 5 (CMIP5). The stabilized
85 global warming pathway is represented by the RCP2.6 low emissions scenario that
86 yields an equilibrium change in Global Mean Temperature (Δ GMT) of 1.49°C by 2050-
87 2070 with selected climate models (Fig. S1). The transient pathway is represented by
88 RCP8.5 high emission scenario in which Δ GMT grows rapidly and realizes a transient
89 1.5°C around the year 2021-2041. We select the present-day period of 1995-2015 as a
90 reference.

91
92

93 **2 Methods**

94 **2.1 Datasets**

95 **2.1.1 CMIP5 data**

96 We use both daily and monthly meteorology predicted by CMIP5 models
97 (<https://cmip.llnl.gov/>). The daily data are used as input for YIBs model. In total, we
98 select 15 climate models (Table S1) with all available daily meteorology, including
99 surface air temperature, precipitation, specific humidity, surface downward shortwave
100 radiation, surface pressure, and surface wind speed, for historical and two future
101 scenarios (RCP2.6 and RCP8.5). These two scenarios assume distinct emission
102 pathways of both CO₂ and air pollutants, with the RCP2.6 scenario projecting much
103 lower CO₂ and pollution concentrations than RCP8.5. Simulated annual GMT is
104 smoothed with a 21-year window to remove decadal variations. The ensemble changes
105 of GMT relative to PI period (1861-1900) from two scenarios are examined (Fig. S1a).
106 The low emission scenario RCP2.6 yields an equilibrium Δ GMT of 1.85°C by 2100.
107 We further remove 8 climate models predicting stabilized Δ GMT higher than 1.85°C
108 by the end of century. The 7 remaining models yield an ensemble warming close to
109 1.5°C (1.49°C for 2050-2070, Fig. S1b). Meanwhile, Δ GMT in the high emission



110 scenario RCP8.5 grows fast and realizes a transient 1.5°C warming around the year
111 2021-2041. Daily meteorology from 7 selected models (Table S1) are then interpolated
112 to the uniform 1°×1° resolution and used to drive YIBs model to simulate terrestrial
113 carbon fluxes in China for 1850-2100. Due to the large data storage, we retain only the
114 domain of [15-60°N, 60-150°E] covering China territory. We bias correct modeled
115 meteorology with WFDEI (WATCH Forcing Data methodology applied to ERA-
116 Interim reanalysis) data (Weedon et al., 2014):

117

$$118 \quad V_d^s = V_d \times S_w / S_m \quad (1)$$

119

120 Here V_d is the original daily variables and V_d^s is the scaled value. S_w is the 2-
121 dimensional WFDEI value averaged for 1980-2004 and S_m is the modeled values
122 averaged at the same period. In this case, the average climate from each individual
123 model matches observations at present day, meanwhile, climate variability from models
124 are retained to estimate uncertainties in carbon fluxes.

125

126 **2.1.2 TRENDY-v6 data**

127 We acquire the global GPP and NEE datasets from 1901 to 2016 simulated by 14
128 Dynamic Global Vegetation Models (DGVMs) participating in TRENDY project
129 (Table S2). All DGVMs are implemented following the same simulation protocol and
130 driven by consistent input datasets, including CRU-NCEP climate data, atmospheric
131 CO₂ concentrations, but fixed present-day land use (Le Quere et al., 2018).

132

133 **2.1.3 ACCMIP O₃ data**

134 We use monthly output of surface O₃ concentrations from 12 models joining the
135 Atmospheric Chemistry and Climate Model Intercomparison Project (ACCMIP,
136 Lamarque et al., 2013) (Table S3). The ACCMIP models have a wide range of
137 horizontal and vertical resolutions, natural emissions, chemistry schemes, and
138 interaction with radiation and clouds. However, they apply the same protocols for
139 anthropogenic and biomass burning emissions specified for CMIP5 RCP scenarios,



140 though different models perform simulations at different time slices. Here, we use
141 surface O₃ and interpolate original output to 1°×1° resolution. We fill the temporal gaps
142 between two adjacent time slices using a linear fitting approach. In this way, we derive
143 the monthly O₃ from 1850 to 2100 for each model and their ensemble average at each
144 grid point.

145

146 **2.1.4 Diffuse radiation data**

147 The original CMIP5 archive does not provide diffuse component of shortwave radiation.
148 Here, we use empirical relations between total and diffuse radiation from 11 studies to
149 calculate hourly diffuse radiation (Table S4). The diffuse fraction k_d in all equations
150 depends on clearness index k_t , which is defined as the ratio between global solar
151 radiation I_t and extra-terrestrial solar radiation I_0 (Ghosh et al., 2017):

$$152 \quad k_t = I_t/I_0 \quad (2)$$

$$153 \quad I_0 = I_{sc} \left[1 + 0.033 \cos\left(\frac{360N}{365}\right) \right] \cos\varphi \quad (3)$$

154 Here $I_{sc} = 1367 \text{ W m}^{-2}$ is solar constant, N is Julian day of the year, and φ is solar zenith.

155 The empirical equations are evaluated using hourly total and diffuse radiation from
156 Modern-Era Retrospective Analysis for Research and Applications (MERRA)
157 (Rienecker et al., 2011) during 2008-2012. For each grid in China, we calculate hourly
158 diffuse radiation (D_c) using MERRA total radiation and compare it with the standard
159 output (D_m). Statistical metrics including correlation, normalized mean bias (NMB),
160 and normalized root mean square error (NRMSE) are used to evaluate the performance
161 of empirical equations:

$$162 \quad \text{NMB} = (\overline{D_c} - \overline{D_m})/\overline{D_m} \quad (4)$$

$$163 \quad \text{NRMSE} = \sqrt{\sum \frac{(D_c - D_m)^2}{n} / \overline{D_m}} \quad (5)$$

164 Here $\overline{D_c}$ and $\overline{D_m}$ are mean values of calculated and MERRA diffuse radiation. The
165 evaluation is performed month by month for 2008-2012 and n is the number of daytime
166 samples (grids with total radiation $> 5 \text{ W m}^{-2}$). The value of n varies from month to
167 month with a minimum of 540,000 in December 2010. Evaluation shows the empirical
168 model M01 (Lam and Li, 1996) yields the highest correlation and the lowest NRMSE



169 (Fig. S2). As a result, we use M01 model to derive diffuse radiation from CMIP5
170 models.

171

172 **2.2 Model**

173 We apply the YIBs model (Yue and Unger, 2015; Yue et al., 2017) to simulate historical
174 and future (1850-2100) ecosystem productivity. The YIBs model dynamically
175 calculates LAI and tree height based on carbon assimilation and allocation. Leaf-level
176 photosynthesis is calculated hourly using the well-established Farquhar et al. (1980)
177 scheme and is upscaled to canopy level by the separation of sunlit and shading leaves
178 (Spitters, 1986). The assimilated carbon is in part used for maintenance and growth
179 respiration, and the rest is allocated among leaf, stem, and root for plant growth (Clark
180 et al., 2011). Soil respiration is calculated as the loss of carbon flows among 12 soil
181 carbon pools (Schaefer et al., 2008). The YIBs model considers 9 plant functional types
182 (PFTs) including evergreen needleleaf forest (ENF), deciduous broadleaf forest (DBF),
183 evergreen broadleaf forest (EBF), shrubland, tundra, C3 grassland, C4 grassland, C3
184 cropland, and C4 cropland. The land cover is prescribed based on satellite retrievals
185 from the Moderate Resolution Imaging Spectroradiometer (MODIS) (Hansen et al.,
186 2003) and the Advanced Very High Resolution Radiometer (AVHRR) (Defries et al.,
187 2000). For this study, we fix the land cover to isolate impacts of CO₂ and climatic
188 changes. Other studies also show only moderate changes in vegetation fraction and
189 composition at a low warming level (Warszawski et al., 2013). The YIBs model can be
190 applied at the site, regional, and global scales. The site-level model has been evaluated
191 with measured carbon fluxes from 145 FLUXNET sites (Yue and Unger, 2015). For
192 this study, all simulations are performed at the 1°×1° resolution over China. During the
193 period of 1982-2011, YIBs predicts an average GPP of 7.17 Pg C yr⁻¹ in China (Fig.
194 S3), close to the 7.25 Pg C yr⁻¹ estimated in the benchmark product (Jung et al., 2009).
195

196 YIBs model calculates O₃ damage to plant photosynthesis using a flux-based
197 parameterization (Sitch et al., 2007). The inhibition rate of GPP is dependent on both
198 ambient O₃ concentrations and stomatal conductance. Compared to hundreds of meta-



199 analyses data from China (Table S5) and the world (Yue and Unger, 2018), the scheme
200 shows good performance in estimating GPP responses to O₃ for DBF, EBF, C3 and C4
201 herbs (Fig. S4). The predicted O₃ damaging effects to ENF might be underestimated.
202 The YIBs model separates the effects of diffuse and direct light on plant photosynthesis
203 (Spitters, 1986). Simulated GPP responses to direct and diffuse radiation show good
204 agreement with observations at 24 global flux tower sites from FLUXNET network
205 (Yue and Unger, 2018).

206

207 **2.3 Simulations**

208 We perform two main groups of simulations, one for RCP2.6 and the other for RCP8.5.
209 For each group, 7 sub-groups are designed with varied climatic or CO₂ forcings (Table
210 S6). In each sub-group, separate runs are conducted for the YIBs model driven with
211 climate variables from 7 selected CMIP5 models (Table S1), making a total of 98 runs.
212 A baseline group (HIST_2000) is performed with fixed meteorology and CO₂ after the
213 year 2000. Another four sub-group simulations are performed to quantify O₃ effects on
214 photosynthesis (Table S7). These simulations are driven with both CMIP5 meteorology
215 and monthly O₃ concentrations from an ensemble of 12 ACCMIP models. The runs are
216 distinguished with different O₃ damaging sensitivity (high or low) and scenario
217 projections (RCP2.6 or RCP8.5). Monthly O₃ concentrations are downscaled to hourly
218 step using the diurnal cycle simulated by a chemistry-climate model NASA ModelE2
219 (Schmidt et al., 2014). The O₃-affected GPP or NEE are calculated as the average of
220 simulations with low and high sensitivities.

221

222 For each run, a 251-year simulation is performed with historical climate for 1850-2000
223 and future climate for 2001-2100. For simulations driven with meteorology from the
224 same climate model, all sensitivity tests apply the same climate forcing during historical
225 period but utilize varied forcings after the year 2000. For example, RCP26_CO2 is
226 identical to RCP26_MET for the period of 1850-2000. However, after the year 2000,
227 the former runs fix climatic conditions at the year 2000 but allow changes in CO₂
228 concentrations year by year for 2001-2100 following the pathway projection, while the



229 latter fix CO₂ level at the year 2000 but continue to use day-to-day meteorology after
230 2000. For all simulations, we initialize vegetation and soil carbon pools in the YIBs
231 model with a 200-year spin up by recycling meteorology at the year of 1850.
232 Contributions of individual factors are calculated as the differences between sensitivity
233 and baseline group (e.g., RCP26_CO2 – HIST_2000 for CO₂ fertilization in RCP2.6
234 scenario).

235

236 **3 Results**

237 **3.1 Changes of atmospheric compositions and radiation**

238 The ensemble concentrations of ACCMIP O₃ show good agreement with ground-based
239 observations from 1580 sites in China (Fig. 1). The spatial correlation is $R=0.80$ ($p <$
240 0.01) between observations and the ensemble O₃ concentrations ($[O_3]$), though the latter
241 is higher by 25% (Figs. 1a-1c). Such overestimation is likely attributed to the high $[O_3]$
242 at night in the models, because the evaluation of maximum daily 8-hour average
243 (MDA8) $[O_3]$, which mainly occurs in the daytime, shows more reasonable predictions
244 with a lower bias of 10% (Figs. 1d-1f). Since the O₃ vegetation damage in general
245 occurs in the daytime, when both plant photosynthesis and $[O_3]$ are at high levels, the
246 ACCMIP $[O_3]$ is good to be used as input for YIBs model to derive long-term O₃
247 inhibition effects on ecosystem productivity.

248

249 The ensemble radiation from CMIP5 models matches observations at 106 sites in China
250 (Fig. 2). For total shortwave radiation, the model prediction shows high values in the
251 West and low values in the Southeast, consistent with observations for a correlation
252 coefficient of $R = 0.79$ ($p < 0.01$) and a mean bias of 8.9%. The derived diffuse radiation
253 is highest in the Southeast, where the total radiation is lowest. Observed diffuse
254 radiation is available only at 17 sites. Compared to these sites, predictions show
255 reasonable spatial distribution with a correlation of $R = 0.65$ ($p < 0.01$) and a low bias
256 of 7.1%. Both the total radiation and derived diffuse radiation are used as input for YIBs
257 model to estimate GPP responses to joint changes in direct and diffuse radiation caused
258 by aerosol removal.



259

260 Atmospheric compositions and radiation show varied changes in different scenarios.
261 The GMT changes mainly follow those in CO₂ concentrations, which show fast growth
262 in RCP8.5 but slow changes in RCP2.6 (Fig. 3a). The latter assumes a large reduction
263 of carbon emissions globally after the year 2020 (Meinshausen et al., 2011). Global
264 CO₂ levels reduce slightly after the year 2030 in RCP2.6, while GMT continues
265 growing until 2050 due to air-sea interactions (Solomon et al., 2009). As a low emission
266 scenario, RCP2.6 experiences a slow growth in nitrogen oxide (NO_x) emissions and a
267 continuous reduction after the year 2020 (Fig. S5), resulting in a decline of 6.4 ppb
268 (15.2%) in surface O₃ over eastern China by 1.5°C warming at 2060 (Fig. 3b). In
269 contrast, RCP8.5 assumes fast growth of NO_x emissions with delayed controls after the
270 year 2030, leading to surface O₃ enhancements of 6.6 ppb (15.7%) by 1.5°C warming
271 at 2030. The lower emissions in RCP2.6 also result in smaller aerosol optical depth
272 (AOD) than RCP8.5 (Fig. S6), leading to higher surface total radiation (Fig. 3c) while
273 lower diffuse radiation (Fig. 3d) due to reducing light extinction (Yu et al., 2006).

274

275 **3.2 Historical ecosystem productivity in China**

276 The ensemble simulations show an increasing trend in gross primary productivity (GPP)
277 in China of 0.011 Pg C yr⁻² over the historical period, 1901-2016 (Fig. 4a). A stronger
278 trend of 0.022 Pg C yr⁻² is found after 1960. Such change is much faster than the trend
279 of 0.013 Pg C yr⁻² estimated by a benchmark product (Jung et al., 2009) for 1982-2011
280 but close to a recent estimate of 0.02 Pg C yr⁻² combining machine learning algorithms
281 and eddy flux measurements from 40 sites in China (Yao et al., 2018). Simulated trend
282 is also consistent with the TRENDY ensemble, which predicts trends of 0.013 ± 0.006
283 Pg C yr⁻² (ensemble ± inter-model uncertainty) for 1901-2016 and 0.022 ± 0.01 Pg C
284 yr⁻² for 1961-2016. The YIBs simulations show variabilities of 0.41±0.23 Pg C yr⁻¹
285 (6.2±3.9%, blue shading in Fig. 4a) due to uncertainties in climate, much smaller than
286 the value of 1.33±0.16 Pg C yr⁻¹ (19.2±2.6%, red shading in Fig. 4a) caused by
287 structural uncertainties across different vegetation models.

288



289 Net ecosystem exchange (NEE) in China is negative, suggesting a regional land carbon
290 sink (Fig. 4b). This sink is moderate at $-46.3 \text{ Tg C yr}^{-1}$ before 1960 but shows a strong
291 trend of $-3.1 \text{ Tg C yr}^{-2}$ thereafter. Such change matches TRENDY simulations, which
292 predict a weak carbon sink of -2 Tg C yr^{-1} before 1960 and a strengthened trend of -
293 $3.2 \pm 2.8 \text{ Tg C yr}^{-2}$ for 1961-2016. However, TRENDY predicts ensemble sources of
294 $41.3 \text{ Tg C yr}^{-1}$ for 1915-1930 and $25.6 \text{ Tg C yr}^{-1}$ for 1980-1989, both of which are
295 missing in the YIBs simulations. For the latter period, the ground-based estimate (Piao
296 et al., 2009) suggests a sink of $177 \pm 73 \text{ Tg C yr}^{-1}$ in China, consistent with the sink
297 intensity of $149 \pm 20 \text{ Tg C yr}^{-1}$ from the YIBs ensemble prediction. For the recent period
298 of 1980-2000, YIBs estimates a strengthened sink of $154 \pm 30 \text{ Tg C yr}^{-1}$ in China, weaker
299 than the estimate of $198 \pm 114 \text{ Tg C yr}^{-1}$ with the DLEM vegetation model (Tian et al.,
300 2011) but is within the estimates of $137\text{-}177 \text{ Tg C yr}^{-1}$ based on both ground and satellite
301 data (Fang et al., 2007). The interannual variability in YIBs simulations is much weaker
302 than the estimates in other studies, because the ensemble approach largely dampen
303 variations among different runs. Similar to GPP, the NEE simulations exhibit smaller
304 variability of $62 \pm 50 \text{ Tg C yr}^{-1}$ among different YIBs runs than that of $128 \pm 88 \text{ Tg C yr}^{-1}$
305 among different TRENDY models.

306

307 **3.3 Future changes of carbon fluxes**

308 For a global warming of 1.5°C , GPP increases significantly in China, especially over
309 eastern and northeastern parts (Fig. 5). Compared to the present day, GPP with O_3
310 effects increases by $1.07 \pm 0.38 \text{ Pg C yr}^{-1}$ ($15.5 \pm 5.4 \%$) in the RCP2.6 scenario (Fig.
311 5a) and $0.82 \pm 0.30 \text{ Pg C yr}^{-1}$ ($11.9 \pm 5.4\%$) in RCP8.5 (Fig. 5b). The spatial pattern of
312 the GPP changes is similar in the two pathways (correlation coefficient $R=0.93$), except
313 that ΔGPP in RCP2.6 is higher than in RCP8.5 by 30% with a positive center over
314 eastern China (Fig. 5c). The NEE changes in China show opposite tendencies between
315 the two pathways. Compared to the present day, a global warming of 1.5°C enhances
316 NEE by $0.03 \pm 0.03 \text{ Pg C yr}^{-1}$ ($-17.4 \pm 19.6 \%$) in RCP2.6 (Fig. 5d) but reduces NEE by
317 $0.14 \pm 0.04 \text{ Pg C yr}^{-1}$ ($94.4 \pm 24.9 \%$) in RCP8.5 (Fig. 5e), suggesting that land carbon
318 sink is slightly weakened in the former but strengthened in the latter. Their differences



319 exhibit widespread positive values in China with high centers in the East (Fig. 5f).
320
321 The changes in carbon fluxes follow the variations in atmospheric composition and
322 climate (Fig. 6 and Figs. S7-S10). By the global warming of 1.5°C, a dominant fraction
323 of GPP enhancement in China is attributed to CO₂ fertilization (Fig. 6a). For the RCP2.6
324 scenario, CO₂ alone contributes 0.83 Pg C yr⁻¹ (77%) to ΔGPP, with the highest
325 enhancement of 0.8 g C m⁻² day⁻¹ over the southeast coast (Fig. S7a). For RCP8.5, CO₂
326 fertilization increases GPP by 0.95 Pg C yr⁻¹, even higher than the total ΔGPP of 0.82
327 Pg C yr⁻¹. The larger CO₂-induced ΔGPP in RCP8.5 is due to the higher CO₂
328 concentrations (454 ppm) than RCP2.6 (442 ppm) at the same 1.5°C warming (Fig. 3a).
329 The 12 ppm differences in CO₂ concentrations lead to a change of 0.12 Pg C yr⁻¹ (1.7%)
330 in GPP. This sensitivity of GPP to CO₂, 0.14% ppm⁻¹, falls within the range of 0.05-
331 0.21% ppm⁻¹ as predicted by 10 terrestrial models (Piao et al., 2013) and that of 0.01-
332 0.32% ppm⁻¹ as observed from multiple free-air CO₂ enrichment (FACE) sites
333 (Ainsworth and Long, 2005). The higher ΔGPP in RCP2.6 instead yields a weakened
334 NEE due to the CO₂ effects (Fig. 6b). The stabilization of CO₂ concentrations in this
335 scenario (Fig. 3a) results in a stabilized GPP, while the 55-year (from 1995-2015 to
336 2050-2070) accumulation of soil carbon continues promoting soil respiration to
337 0.71±0.19 Pg C yr⁻¹, much higher than the value of 0.41±0.15 Pg C yr⁻¹ in RCP8.5 from
338 the 26-year (to 2021-2041) carbon uptake. The continuous increase of CO₂ and lower
339 soil respiration jointly strengthen the land carbon sink in China by 0.1 Pg C yr⁻¹ under
340 RCP8.5 scenario (Fig. 6a).
341
342 Ozone (O₃) damages plant photosynthesis and the land carbon sink (Sitch et al.,
343 2007; Yue and Unger, 2018). In the present day, O₃ decreases GPP by 6.7% in China
344 (Fig. 7d), because of the direct inhibition of photosynthesis by 6% (Fig. 7a) and the
345 consequent reduction of 1.8% in leaf area index (LAI, Fig. 7g). For 1.5°C global
346 warming, this weakening effect shows opposite tendencies in the two RCP scenarios,
347 with a reduced GPP loss of 4.7% in RCP2.6 (Fig. 7e) but an increased loss of 7.9% in
348 RCP8.5 (Fig. 7f). These impacts are predominantly driven by the variations of surface



349 O₃ concentrations in the two scenarios, as predicted O₃ at 1.5°C warming decreases by
350 15.2% in the low emission pathway but increases by 15.7% in the high emission
351 pathway (Fig. 3b). Consequently, changes in O₃ help increase GPP by 0.1 Pg C yr⁻¹ in
352 RCP2.6 but decrease GPP by 0.14 Pg C yr⁻¹ in RCP8.5 for the same 1.5°C warming.
353 Following the benefits to GPP, the lower O₃ decreases NEE (strengthens the sink) by
354 0.06 Pg C yr⁻¹ in RCP2.6, offsetting more than half of the negative effect (weakens the
355 sink) from CO₂ (Fig. 6b). For RCP8.5, O₃ impacts make limited contributions to ΔNEE.
356

357 Changes in meteorology account for the rest of the perturbations in the carbon fluxes.
358 At the global warming of 1.5°C, temperature in China increases by 0.90°C for RCP2.6
359 and 0.91°C for RCP8.5 (Figs. S11a-S11b) compared to present-day climate. The spatial
360 pattern of these changes is very similar without significant differences (Fig. S11c),
361 leading to almost identical GPP responses (Figs. S7d and S8d). Generally, higher
362 temperature is not beneficial for plant photosynthesis at low latitudes (Piao et al., 2013),
363 where regional summer climate is already warmer than the optimal temperature
364 threshold for leaf photosynthesis (Corlett, 2011). As a result, warming leads to negative
365 changes in GPP over the East. Surface specific humidity exhibits widespread
366 enhancement in eastern China (Figs. S12a-S12b). Air humidity may rise in a warmer
367 climate because the corresponding enhancement of saturation pressure allow
368 atmosphere to hold more water vapor. On average, surface specific humidity increases
369 by 0.34 g kg⁻¹ in RCP2.6 and 0.31 g kg⁻¹ in RCP8.5, leading to a promotion of GPP by
370 0.14 Pg C yr⁻¹ in the former and a similar value of 0.12 Pg C yr⁻¹ in the latter (Figs. S7e
371 and S8e). Precipitation increases by 0.14 mm day⁻¹ (4.6%) over eastern China in
372 RCP2.6 but decreases by 0.03 mm day⁻¹ (1.2%) in RCP8.5 (Figs. S11d-S11e), leading
373 to higher soil moisture in eastern China for RCP2.6 (Figs. S12d-S12e). Nevertheless,
374 most of vegetation in eastern China is not water stressed, leaving moderate GPP
375 responses to soil moisture changes in both RCP scenarios (Figs. S7f and S8f).
376

377 For the RCP2.6 scenario, the net effect of climate change causes an increase of 0.15 Pg
378 C yr⁻¹ in GPP with a range from -0.54 to 0.62 Pg C yr⁻¹ (Fig. 6a). Such large variability



379 in Δ GPP is related to the uncertainties in meteorology from different climate models.
380 For RCP8.5, climate-induced GPP change is only $0.04 \text{ Pg C yr}^{-1}$ with a range from -0.6
381 to $0.26 \text{ Pg C yr}^{-1}$. The discrepancy of Δ GPP for the two pathways is mainly caused by
382 the different radiation impacts, which enhance GPP by 0.2 Pg C yr^{-1} in RCP2.6 but only
383 $0.11 \text{ Pg C yr}^{-1}$ in RCP8.5 (Fig. 6a). Photosynthetically active radiation (PAR) is higher
384 by 2.8 W m^{-2} in RCP2.6 than in RCP8.5 (Fig. 3c). The distinct changes in radiation are
385 related to aerosol radiative effects, because global analyses also show radiation
386 enhancement in regions (e.g., U.S. and Europe) with aerosol removal (Fig. S13). The
387 lower AOD in RCP2.6 helps increase solar insolation at surface by reducing light
388 extinction (Yu et al., 2006), and promote precipitation with weaker aerosol semi-direct
389 and indirect effects (Lohmann and Feichter, 2005). Although lower aerosols in RCP2.6
390 slightly decrease diffuse radiation (Fig. 3d), which is more efficient in increasing
391 photosynthesis (Mercado et al., 2009; Yue and Unger, 2018), the overall enhancement
392 in total radiation helps boost GPP. Climate-induced Δ NEE is $-0.02 \text{ Pg C yr}^{-1}$ for both
393 pathways (Fig. 6b), resulting from comparable responses of NEE to changes in
394 radiation ($R=0.82$), temperature ($R=0.71$), air humidity ($R=0.91$), and soil moisture
395 ($R=0.73$) between the two pathways (Figs. S9 and S10).

396

397 **3.4 Impacts on allowable carbon budget**

398 For a warming target of 1.5°C , our analyses suggest that a simultaneous reduction of
399 CO_2 and air pollution emissions is better for land carbon uptake than a pathway without
400 air pollution emission control. The increased light availability from aerosol removal
401 and decreased surface O_3 jointly promote GPP in China by 0.3 Pg C yr^{-1} , equivalent to
402 36% of the CO_2 fertilization. In contrast, air pollution results in a net GPP inhibition of
403 $0.03 \text{ Pg C yr}^{-1}$ under the high emission pathway, suggesting a detrimental environment
404 for plant health. Compared to RCP8.5, the timing of 1.5°C warming is delayed by 30
405 years in RCP2.6, leading to weaker carbon sink in the latter. However, even with the
406 longer period of accumulation, the total carbon loss by O_3 damage is smaller by 3-16%
407 in RCP2.6 relative to RCP8.5 at the same warming level (Fig. 8a).

408



409 The slow warming increases the allowable cumulative anthropogenic carbon emissions.
410 Assuming China's carbon emission fraction of 27% of the world (the level at year 2017)
411 (Le Quere et al., 2018), the total national emissions allowed are 80.4 Pg C in RCP2.6
412 and 71.9 Pg C in RCP8.5 from the year 2010 to the 1.5°C warming, following the global
413 emission rates defined for these scenarios. The ensemble simulations show that
414 ecosystems in China help mitigate 8.5 ± 1.1 Pg C in RCP2.6 and 4.5 ± 0.6 Pg C in RCP8.5
415 (Fig. 8b). Sensitivity experiments with either reduced CO₂ (but retain high pollution)
416 or reduced pollution (but retain high CO₂) reveal land carbon uptakes of 7.3 ± 0.9 Pg C
417 and 5.0 ± 0.6 Pg C, respectively. These values are both lower than that in RCP2.6,
418 suggesting that simultaneous control of carbon and air pollution emissions can
419 maximize the mitigation potential of ecosystems. The higher ecosystem assimilation
420 rate in a low emission pathway ($10.6 \pm 1.4\%$ in RCP2.6 vs. $6.3 \pm 0.8\%$ in RCP8.5) over
421 China, which is not considered in CMIP5 models, further buffers the pace to the global
422 warming of 1.5°C.

423

424 **4 Discussion and conclusions**

425 Projection of future ecosystem productivity is subject to uncertainties in climate forcing
426 and biophysical responses. The multi-model ensemble is a good approach to reduce the
427 uncertainty in climate (Flato et al., 2013). In this study, we employ daily meteorology
428 from 7 CMIP5 models. A comparison with more CMIP5 models is performed (not
429 shown) and confirms that the changes in meteorology from the 7 selected climate
430 models are robust and representative of future projections. As for ecosystem responses,
431 future projections generally showed increasing GPP in China (Ju et al., 2007; Ji et al.,
432 2008; Mu et al., 2008), however, climate change alone usually reduces productivity by
433 inducing hot and drought weather conditions. In contrast, the YIBs simulations reveal
434 a net positive effect of climate change on GPP though with large uncertainties (Fig. 6a).
435 Such discrepancies are related to structural uncertainties across different vegetation
436 models. Evaluations suggest that biophysical responses to environmental forcings in
437 the YIBs model are generally reasonable as compared to the TRENDY ensemble (Fig.
438 4).



439

440 The YIBs simulations do not consider nitrogen cycle and its limitation on carbon uptake.
441 Inter-model comparisons show that models without nutrient constraints tend to
442 overestimate GPP responses to CO₂ fertilization (Smith et al., 2016). As a result, the
443 difference of CO₂ contributions in RCP scenarios would be smaller than predicted (Fig.
444 6a), suggesting that GPP enhancement in RCP2.6 might be even higher than RCP8.5 if
445 nitrogen cycle is included. In contrast, nitrogen deposition in RCP2.6 would be much
446 smaller than that in RCP8.5 due to emission control (Fig. S5), leading to lower nitrogen
447 supply for ecosystem in the former scenario. Consequently, plant photosynthesis is
448 confronted with stronger nutrient limit in RCP2.6 than that in RCP8.5, resulting in
449 lower CO₂ fertilization efficiency in the former scenario. The net effect of nitrogen
450 cycle on land carbon cycle is very uncertain (Zaehle et al., 2014;Xiao et al.,
451 2015;Huntzinger et al., 2017).

452

453 For a warming target of 1.5°C, our analyses suggest that an associated reduction of CO₂
454 and pollution emissions brings more benefits to ecosystems in China than a pathway
455 without emission control. The slow changes of temperature and other environmental
456 variables due to slow growth of CO₂ are helpful for plant adaptation and limit biome
457 shift (Warszawski et al., 2013), and the lower O₃ and higher solar radiation from aerosol
458 removal increase plant photosynthesis. Consequently, China's ecosystems mitigate
459 10.6±1.4% of national emissions in the stabilized pathway, more efficient than the
460 fraction of 6.3±0.8% in the transient pathway, leaving more allowable carbon budget
461 for economic development and upgrade.

462

463

464

465



466 **References**

- 467 Ainsworth, E. A., and Long, S. P.: What have we learned from 15 years of free-air CO₂ enrichment
468 (FACE)? A meta-analytic review of the responses of photosynthesis, canopy, *New Phytol*, 165, 351-
469 371, 10.1111/J.1469-8137.2004.01224.X, 2005.
- 470 Burke, M., Davis, W. M., and Diffenbaugh, N. S.: Large potential reduction in economic damages under
471 UN mitigation targets, *Nature*, 557, 549-553, 10.1038/s41586-018-0071-9, 2018.
- 472 Clark, D. B., Mercado, L. M., Sitch, S., Jones, C. D., Gedney, N., Best, M. J., Pryor, M., Rooney, G. G.,
473 Essery, R. L. H., Blyth, E., Boucher, O., Harding, R. J., Huntingford, C., and Cox, P. M.: The Joint
474 UK Land Environment Simulator (JULES), model description - Part 2: Carbon fluxes and
475 vegetation dynamics, *Geosci Model Dev*, 4, 701-722, 10.5194/Gmd-4-701-2011, 2011.
- 476 Collins, W. J., Webber, C. P., Cox, P. M., Huntingford, C., Lowe, J., Sitch, S., Chadburn, S. E., Comyn-
477 Platt, E., Harper, A. B., Hayman, G., and Powell, T.: Increased importance of methane reduction for
478 a 1.5 degree target, *Environ Res Lett*, 13, 054003, 10.1088/1748-9326/aab89c, 2018.
- 479 Corlett, R. T.: Impacts of warming on tropical lowland rainforests, *Trends Ecol Evol*, 26, 606-613,
480 10.1016/j.tree.2011.06.015, 2011.
- 481 Dai, E. F., Wu, Z., Ge, Q. S., Xi, W. M., and Wang, X. F.: Predicting the responses of forest distribution
482 and aboveground biomass to climate change under RCP scenarios in southern China, *Global Change
483 Biol*, 22, 3642-3661, 10.1111/gcb.13307, 2016.
- 484 Defries, R. S., Hansen, M. C., Townshend, J. R. G., Janetos, A. C., and Loveland, T. R.: A new global 1-
485 km dataset of percentage tree cover derived from remote sensing, *Global Change Biol*, 6, 247-254,
486 10.1046/J.1365-2486.2000.00296.X, 2000.
- 487 Fang, J. Y., Guo, Z. D., Piao, S. L., and Chen, A. P.: Terrestrial vegetation carbon sinks in China, 1981-
488 2000, *Sci China Ser D*, 50, 1341-1350, 10.1007/s11430-007-0049-1, 2007.
- 489 Fang, J. Y., Shen, Z. H., Tang, Z. Y., Wang, X. P., Wang, Z. H., Feng, J. M., Liu, Y. N., Qiao, X. J., Wu,
490 X. P., and Zheng, C. Y.: Forest community survey and the structural characteristics of forests in
491 China, *Ecography*, 35, 1059-1071, 10.1111/j.1600-0587.2013.00161.x, 2012.
- 492 Farquhar, G. D., Caemmerer, S. V., and Berry, J. A.: A Biochemical-Model of Photosynthetic Co₂
493 Assimilation in Leaves of C-3 Species, *Planta*, 149, 78-90, 10.1007/Bf00386231, 1980.
- 494 Flato, G., Marotzke, J., Abiodun, B., Braconnot, P., Chou, S. C., Collins, W., Cox, P., Driouech, F., Emori,
495 S., Eyring, V., Forest, C., Gleckler, P., Guilyardi, E., Jakob, C., Kattsov, V., Reason, C., and
496 Rummukainen, M.: Evaluation of Climate Models, in: *Climate Change 2013: The Physical Science
497 Basis. Contribution of Working Group I to the Fifth Assessment Report of the Intergovernmental
498 Panel on Climate Change*, edited by: Stocker, T. F., Qin, D., Plattner, G. K., Tignor, M., Allen, S.
499 K., Boschung, J., Nauels, A., Xia, Y., Bex, V., and Midgley, P. M., Cambridge University Press,
500 Cambridge, United Kingdom and New York, NY, USA, 2013.
- 501 Ghosh, A., Norton, B., and Duffy, A.: Effect of sky clearness index on transmission of evacuated (vacuum)
502 glazing, *Renewable Energy*, 105, 160-166, 10.1016/j.renene.2016.12.056, 2017.
- 503 Hansen, M. C., DeFries, R. S., Townshend, J. R. G., Carroll, M., Dimiceli, C., and Sohlberg, R. A.:



- 504 Global Percent Tree Cover at a Spatial Resolution of 500 Meters: First Results of the MODIS
505 Vegetation Continuous Fields Algorithm, *Earth Interact*, 7, 1-15, 10.1175/1087-
506 3562(2003)007<0001:GPTCAA>2.0.CO;2, 2003.
- 507 He, N. P., Wen, D., Zhu, J. X., Tang, X. L., Xu, L., Zhang, L., Hu, H. F., Huang, M., and Yu, G. R.:
508 Vegetation carbon sequestration in Chinese forests from 2010 to 2050, *Global Change Biol*, 23,
509 1575-1584, 10.1111/gcb.13479, 2017.
- 510 Huntzinger, D. N., Michalak, A. M., Schwalm, C., Ciais, P., King, A. W., Fang, Y., Schaefer, K., Wei, Y.,
511 Cook, R. B., Fisher, J. B., Hayes, D., Huang, M., Ito, A., Jain, A. K., Lei, H., Lu, C., Maignan, F.,
512 Mao, J., Parazoo, N., Peng, S., Poulter, B., Ricciuto, D., Shi, X., Tian, H., Wang, W., Zeng, N., and
513 Zhao, F.: Uncertainty in the response of terrestrial carbon sink to environmental drivers undermines
514 carbon-climate feedback predictions, *Scientific Reports*, 7, 4765, 10.1038/s41598-017-03818-2,
515 2017.
- 516 Ji, J. J., Huang, M., and Li, K. R.: Prediction of carbon exchanges between China terrestrial ecosystem
517 and atmosphere in 21st century, *Sci China Ser D*, 51, 885-898, 10.1007/s11430-008-0039-y, 2008.
- 518 Ju, W. M., Chen, J. M., Harvey, D., and Wang, S.: Future carbon balance of China's forests under climate
519 change and increasing CO₂, *J Environ Manage*, 85, 538-562, 10.1016/j.jenvman.2006.04.028, 2007.
- 520 Jung, M., Reichstein, M., and Bondeau, A.: Towards global empirical upscaling of FLUXNET eddy
521 covariance observations: validation of a model tree ensemble approach using a biosphere model,
522 *Biogeosciences*, 6, 2001-2013, 10.5194/bg-6-2001-2009, 2009.
- 523 Lam, J. C., and Li, D. H. W.: Correlation between global solar radiation and its direct and diffuse
524 components, *Build Environ*, 31, 527-535, 10.1016/0360-1323(96)00026-1, 1996.
- 525 Lamarque, J. F., Shindell, D. T., Josse, B., Young, P. J., Cionni, I., Eyring, V., Bergmann, D., Cameron-
526 Smith, P., Collins, W. J., Doherty, R., Dalsoren, S., Faluvegi, G., Folberth, G., Ghan, S. J., Horowitz,
527 L. W., Lee, Y. H., MacKenzie, I. A., Nagashima, T., Naik, V., Plummer, D., Righi, M., Rumbold, S.
528 T., Schulz, M., Skeie, R. B., Stevenson, D. S., Strode, S., Sudo, K., Szopa, S., Voulgarakis, A., and
529 Zeng, G.: The Atmospheric Chemistry and Climate Model Intercomparison Project (ACCMIP):
530 overview and description of models, simulations and climate diagnostics, *Geosci Model Dev*, 6,
531 179-206, 10.5194/gmd-6-179-2013, 2013.
- 532 Le Quere, C., Andrew, R. M., Friedlingstein, P., Sitch, S., Pongratz, J., Manning, A. C., Korsbakken, J.
533 I., Peters, G. P., Canadell, J. G., Jackson, R. B., Boden, T. A., Tans, P. P., Andrews, O. D., Arora, V.
534 K., Bakker, D. C. E., Barbero, L., Becker, M., Betts, R. A., Bopp, L., Chevallier, F., Chini, L. P.,
535 Ciais, P., Cosca, C. E., Cross, J., Currie, K., Gasser, T., Harris, I., Hauck, J., Haverd, V., Houghton,
536 R. A., Hunt, C. W., Hurtt, G., Ilyina, T., Jain, A. K., Kato, E., Kautz, M., Keeling, R. F., Goldewijk,
537 K. K., Kortzinger, A., Landschutzer, P., Lefevre, N., Lenton, A., Lienert, S., Lima, I., Lombardozi,
538 D., Metzl, N., Millero, F., Monteiro, P. M. S., Munro, D. R., Nabel, J. E. M. S., Nakaoka, S., Nojiri,
539 Y., Padin, X. A., Pregon, A., Pfiel, B., Pierrot, D., Poulter, B., Rehder, G., Reimer, J., Rodenbeck,
540 C., Schwinger, J., Seferian, R., Skjelvan, I., Stocker, B. D., Tian, H. Q., Tilbrook, B., Tubiello, F.
541 N., van der Laan-Luijkx, I. T., van der Werf, G. R., van Heuven, S., Viovy, N., Vuichard, N., Walker,
542 A. P., Watson, A. J., Wiltshire, A. J., Zaehle, S., and Zhu, D.: Global Carbon Budget 2017, *Earth*



- 543 Syst Sci Data, 10, 405-448, 10.5194/essd-10-405-2018, 2018.
- 544 Lohmann, U., and Feichter, J.: Global indirect aerosol effects: a review, *Atmospheric Chemistry and*
545 *Physics*, 5, 715-737, 2005.
- 546 Mann, M. E., Miller, S. K., Rahmstorf, S., Steinman, B. A., and Tingley, M.: Record temperature streak
547 bears anthropogenic fingerprint, *Geophys Res Lett*, 44, 7936-7944, 10.1002/2017gl074056, 2017.
- 548 Meinshausen, M., Smith, S. J., Calvin, K., Daniel, J. S., Kainuma, M. L. T., Lamarque, J. F., Matsumoto,
549 K., Montzka, S. A., Raper, S. C. B., Riahi, K., Thomson, A., Velders, G. J. M., and van Vuuren, D.
550 P. P.: The RCP greenhouse gas concentrations and their extensions from 1765 to 2300, *Climatic*
551 *Change*, 109, 213-241, 10.1007/S10584-011-0156-Z, 2011.
- 552 Mengis, N., Partanen, A.-I., Jalbert, J., and Matthews, H. D.: 1.5 °C carbon budget dependent on carbon
553 cycle uncertainty and future non-CO₂ forcing, *Scientific Reports*, 8, 5831, 2018.
- 554 Mercado, L. M., Bellouin, N., Sitch, S., Boucher, O., Huntingford, C., Wild, M., and Cox, P. M.: Impact
555 of changes in diffuse radiation on the global land carbon sink, *Nature*, 458, 1014-U1087,
556 10.1038/Nature07949, 2009.
- 557 Millar, R. J., Fuglestedt, J. S., Friedlingstein, P., Rogelj, J., Grubb, M. J., Matthews, H. D., Skeie, R. B.,
558 Forster, P. M., Frame, D. J., and Allen, A. R.: Emission budgets and pathways consistent with
559 limiting warming to 1.5 degrees C, *Nat Geosci*, 10, 741-747, 10.1038/Ngeo3031, 2017.
- 560 Mitchell, D., Heavyside, C., Schaller, N., Allen, M., Ebi, K. L., Fischer, E. M., Gasparrini, A., Harrington,
561 L., Kharin, V., Shiogama, H., Sillmann, J., Sippel, S., and Vardoulakis, S.: Extreme heat-related
562 mortality avoided under Paris Agreement goals, *Nat Clim Change*, 8, 551-553, 10.1038/s41558-
563 018-0210-1, 2018.
- 564 Mu, Q. Z., Zhao, M. S., Running, S. W., Liu, M. L., and Tian, H. Q.: Contribution of increasing CO₂(2)
565 and climate change to the carbon cycle in China's ecosystems, *J Geophys Res-Bioge*, 113, G01018,
566 10.1029/2006jg000316, 2008.
- 567 Nangombe, S., Zhou, T., Zhang, W., Wu, B., Hu, S., Zou, L., and Li, D.: Record-breaking climate
568 extremes in Africa under stabilized 1.5°C and 2°C global warming scenarios, *Nat Clim Change*, 8,
569 375-380, 10.1038/s41558-018-0145-6, 2018.
- 570 Piao, S. L., Fang, J. Y., Ciais, P., Peylin, P., Huang, Y., Sitch, S., and Wang, T.: The carbon balance of
571 terrestrial ecosystems in China, *Nature*, 458, 1009-U1082, 10.1038/nature07944, 2009.
- 572 Piao, S. L., Sitch, S., Ciais, P., Friedlingstein, P., Peylin, P., Wang, X. H., Ahlstrom, A., Anav, A.,
573 Canadell, J. G., Cong, N., Huntingford, C., Jung, M., Levis, S., Levy, P. E., Li, J. S., Lin, X., Lomas,
574 M. R., Lu, M., Luo, Y. Q., Ma, Y. C., Myneni, R. B., Poulter, B., Sun, Z. Z., Wang, T., Viovy, N.,
575 Zaehle, S., and Zeng, N.: Evaluation of terrestrial carbon cycle models for their response to climate
576 variability and to CO₂ trends, *Global Change Biol*, 19, 2117-2132, 10.1111/Gcb.12187, 2013.
- 577 Rienecker, M. M., Suarez, M. J., Gelaro, R., Todling, R., Bacmeister, J., Liu, E., Bosilovich, M. G.,
578 Schubert, S. D., Takacs, L., Kim, G. K., Bloom, S., Chen, J. Y., Collins, D., Conaty, A., Da Silva,
579 A., Gu, W., Joiner, J., Koster, R. D., Lucchesi, R., Molod, A., Owens, T., Pawson, S., Pegion, P.,
580 Redder, C. R., Reichle, R., Robertson, F. R., Ruddick, A. G., Sienkiewicz, M., and Woollen, J.:
581 MERRA: NASA's Modern-Era Retrospective Analysis for Research and Applications, *J Climate*,



- 582 24, 3624-3648, 10.1175/Jcli-D-11-00015.1, 2011.
- 583 Schaefer, K., Collatz, G. J., Tans, P., Denning, A. S., Baker, I., Berry, J., Prihodko, L., Suits, N., and
584 Philpott, A.: Combined Simple Biosphere/Carnegie-Ames-Stanford Approach terrestrial carbon
585 cycle model, *J. Geophys. Res.*, 113, G03034, 10.1029/2007jg000603, 2008.
- 586 Schmidt, G. A., Kelley, M., Nazarenko, L., Ruedy, R., Russell, G. L., Aleinov, I., Bauer, M., Bauer, S.
587 E., Bhat, M. K., Bleck, R., Canuto, V., Chen, Y. H., Cheng, Y., Clune, T. L., Del Genio, A., de
588 Fainchtein, R., Faluvegi, G., Hansen, J. E., Healy, R. J., Kiang, N. Y., Koch, D., Lacis, A. A.,
589 LeGrande, A. N., Lerner, J., Lo, K. K., Matthews, E. E., Menon, S., Miller, R. L., Oinas, V., Olosa,
590 A. O., Perlwitz, J. P., Puma, M. J., Putman, W. M., Rind, D., Romanou, A., Sato, M., Shindell, D.
591 T., Sun, S., Syed, R. A., Tausnev, N., Tsigaridis, K., Unger, N., Voulgarakis, A., Yao, M. S., and
592 Zhang, J. L.: Configuration and assessment of the GISS ModelE2 contributions to the CMIP5
593 archive, *J Adv Model Earth Sy*, 6, 141-184, 10.1002/2013ms000265, 2014.
- 594 Stith, S., Cox, P. M., Collins, W. J., and Huntingford, C.: Indirect radiative forcing of climate change
595 through ozone effects on the land-carbon sink, *Nature*, 448, 791-794, 10.1038/Nature06059, 2007.
- 596 Smith, W. K., Reed, S. C., Cleveland, C. C., Ballantyne, A. P., Anderegg, W. R. L., Wieder, W. R., Liu,
597 Y. Y., and Running, S. W.: Large divergence of satellite and Earth system model estimates of global
598 terrestrial CO₂ fertilization, *Nat Clim Change*, 6, 306-310, 10.1038/Nclimate2879, 2016.
- 599 Solomon, S., Plattner, G.-K., Knutti, R., and Friedlingstein, P.: Irreversible climate change due to carbon
600 dioxide emissions, *P Natl Acad Sci USA*, 106, 1704-1709, 10.1073/pnas.0812721106, 2009.
- 601 Spitters, C. J. T.: Separating the Diffuse and Direct Component of Global Radiation and Its Implications
602 for Modeling Canopy Photosynthesis .2. Calculation of Canopy Photosynthesis, *Agr Forest*
603 *Meteorol*, 38, 231-242, 10.1016/0168-1923(86)90061-4, 1986.
- 604 Tian, H. Q., Xu, X. F., Lu, C. Q., Liu, M. L., Ren, W., Chen, G. S., Melillo, J., and Liu, J. Y.: Net
605 exchanges of CO₂, CH₄, and N₂O between China's terrestrial ecosystems and the atmosphere and
606 their contributions to global climate warming, *Journal of Geophysical Research*, 116, G02011,
607 10.1029/2010jg001393, 2011.
- 608 Warszawski, L., Friend, A., Ostberg, S., Frieler, K., Lucht, W., Schaphoff, S., Beerling, D., Cadule, P.,
609 Ciais, P., Clark, D. B., Kahana, R., Ito, A., Keribin, R., Kleidon, A., Lomas, M., Nishina, K., Pavlick,
610 R., Rademacher, T. T., Buechner, M., Piontek, F., Schewe, J., Serdeczny, O., and Schellnhuber, H.
611 J.: A multi-model analysis of risk of ecosystem shifts under climate change, *Environ Res Lett*, 8,
612 044018, 10.1088/1748-9326/8/4/044018, 2013.
- 613 Weedon, G. P., Balsamo, G., Bellouin, N., Gomes, S., Best, M. J., and Viterbo, P.: The WFDEI
614 meteorological forcing data set: WATCH Forcing Data methodology applied to ERA-Interim
615 reanalysis data, *Water Resources Research*, 50, 7505-7514, 10.1002/2014wr015638, 2014.
- 616 Wu, S., Yin, Y., Zhao, D., Huang, M., Shao, X., and Dai, E.: Impact of future climate change on terrestrial
617 ecosystems in China, *International Journal of Climatology*, 30, 866-873, 10.1002/joc.1938, 2009.
- 618 Xiao, J. F., Zhou, Y., and Zhang, L.: Contributions of natural and human factors to increases in vegetation
619 productivity in China, *Ecosphere*, 6, 233, 10.1890/Es14-00394.1, 2015.
- 620 Yao, Y. T., Wang, X. H., Li, Y., Wang, T., Shen, M. G., Du, M. Y., He, H. L., Li, Y. N., Luo, W. J., Ma,



- 621 M. G., Ma, Y. M., Tang, Y. H., Wang, H. M., Zhang, X. Z., Zhang, Y. P., Zhao, L., Zhou, G. S., and
622 Piao, S. L.: Spatiotemporal pattern of gross primary productivity and its covariation with climate in
623 China over the last thirty years, *Global Change Biol*, 24, 184-196, 10.1111/gcb.13830, 2018.
- 624 Yu, H., Kaufman, Y. J., Chin, M., Feingold, G., Remer, L. A., Anderson, T. L., Balkanski, Y., Bellouin,
625 N., Boucher, O., Christopher, S., DeCola, P., Kahn, R., Koch, D., Loeb, N., Reddy, M. S., Schulz,
626 M., Takemura, T., and Zhou, M.: A review of measurement-based assessments of the aerosol direct
627 radiative effect and forcing, *Atmos. Chem. Phys.*, 6, 613-666, 2006.
- 628 Yue, X., and Unger, N.: The Yale Interactive terrestrial Biosphere model: description, evaluation and
629 implementation into NASA GISS ModelE2, *Geosci Model Dev*, 8, 2399-2417, 10.5194/gmd-8-
630 2399-2015, 2015.
- 631 Yue, X., Unger, N., Harper, K., Xia, X., Liao, H., Zhu, T., Xiao, J., Feng, Z., and Li, J.: Ozone and haze
632 pollution weakens net primary productivity in China, *Atmospheric Chemistry and Physics*, 17,
633 6073-6089, 10.5194/acp-17-6073-2017, 2017.
- 634 Yue, X., and Unger, N.: Fire air pollution reduces global terrestrial productivity, *Nat Commun*, 9, 5413,
635 10.1038/s41467-018-07921-4, 2018.
- 636 Zaehle, S., Medlyn, B. E., De Kauwe, M. G., Walker, A. P., Dietze, M. C., Hickler, T., Luo, Y. Q., Wang,
637 Y. P., El-Masri, B., Thornton, P., Jain, A., Wang, S. S., Warlind, D., Weng, E. S., Parton, W., Iversen,
638 C. M., Gallet-Budynek, A., McCarthy, H., Finzi, A. C., Hanson, P. J., Prentice, I. C., Oren, R., and
639 Norby, R. J.: Evaluation of 11 terrestrial carbon-nitrogen cycle models against observations from
640 two temperate Free-Air CO₂ Enrichment studies, *New Phytol*, 202, 803-822, 10.1111/Nph.12697,
641 2014.

642

643

644 **Author Contributions**

645 X.Y., H.L., and H.W. designed the research and wrote the manuscript. X.Y. downloaded CMIP5
646 data, set up models, and performed all simulations. T.Z. evaluated diffuse radiation models. N.U.
647 provided ACCMIP data. S.S. provided TRENDY data. Z.F. provided O₃ damaging meta-analysis
648 data in China. J.Y. analyzed TRENDY results over China. All authors contributed to the
649 interpretation of the results and improvement of the paper.

650

651 **Acknowledgements**

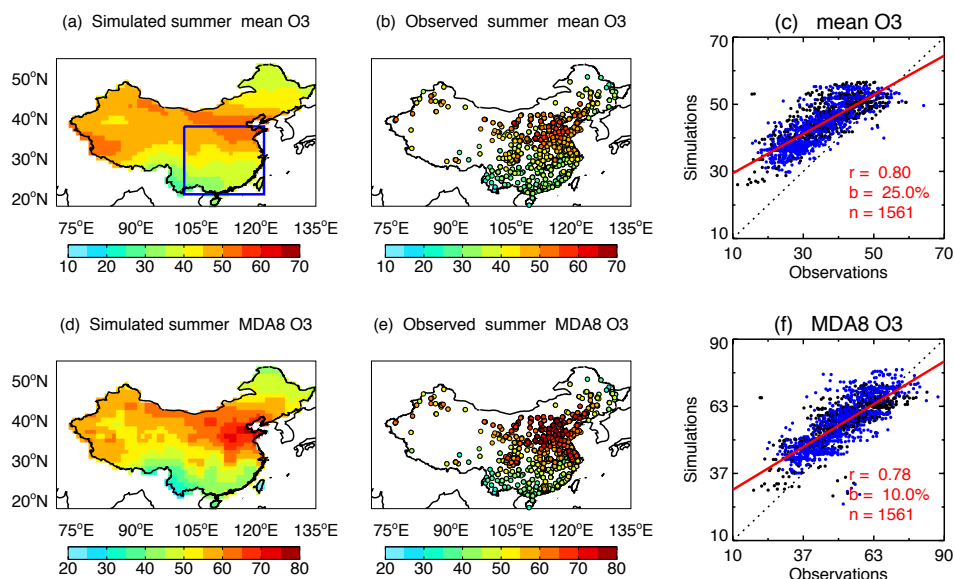
652 This work is supported by the National Key Research and Development Program of China (grant
653 no. 2017YFA0603802) and National Natural Science Foundation of China (grant no. 91744311).

654

655



656

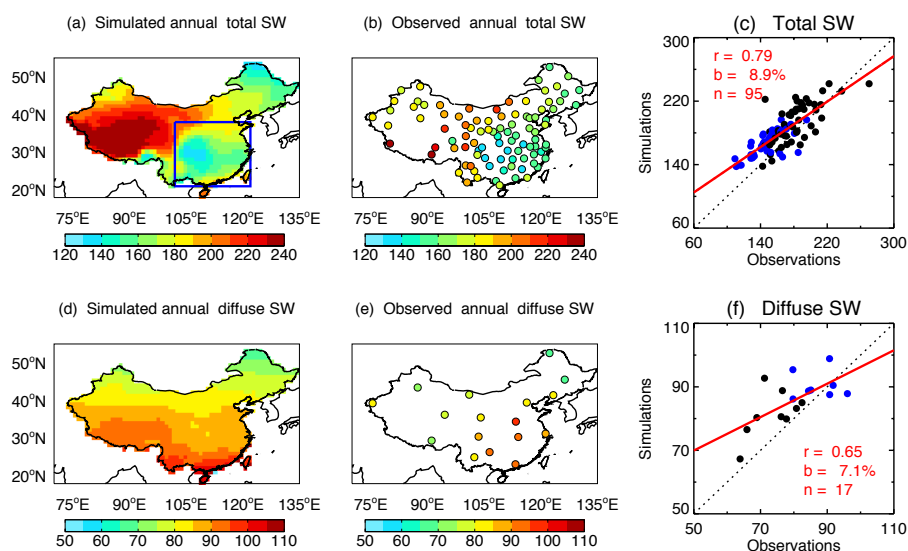


657

658 **Figure 1.** Evaluation of surface O₃ with site-level observations. Simulations are ensemble (a) mean
659 and (d) daily maximum 8-hour average (MDA8) O₃ for the period of 2005-2015 from 12 ACCMIP
660 models. Observations (b and e) are the average during 2015-2018 from 1580 sites operated by
661 Ministry of Ecology and Environment, China. The correlation coefficients (r), relative biases (b),
662 and number of sites (n , excluding data-missing sites) are shown in the scatter plots (c and f). The
663 blue points in the scatter plots represent sites located within the box regions in eastern China as
664 shown in (a). The dashed line represents the 1:1 ratio. The red line is the linear regression between
665 simulations and observations.

666

667



668
669 **Figure 2.** Evaluation of radiation fluxes with site-level observations. Simulations are surface (a)
670 total shortwave radiation (W m^{-2}) and (d) diffuse radiation derived with method M01 (Table S4) for
671 the period of 2005-2015 from an ensemble of 7 CMIP5 climate models. Observations (b and e) are
672 the average during 2009-2011 from 106 sites operated by the Climate Data Center, Chinese
673 Meteorological Administration. The correlation coefficients (r), relative biases (b), and number of
674 sites (n , excluding data-missing sites) are shown in the scatter plots (c and f). The blue points in the
675 scatter plots represent sites located within the box regions in eastern China as shown in (a). The
676 dashed line represents the 1:1 ratio. The red line is the linear regression between simulations and
677 observations.

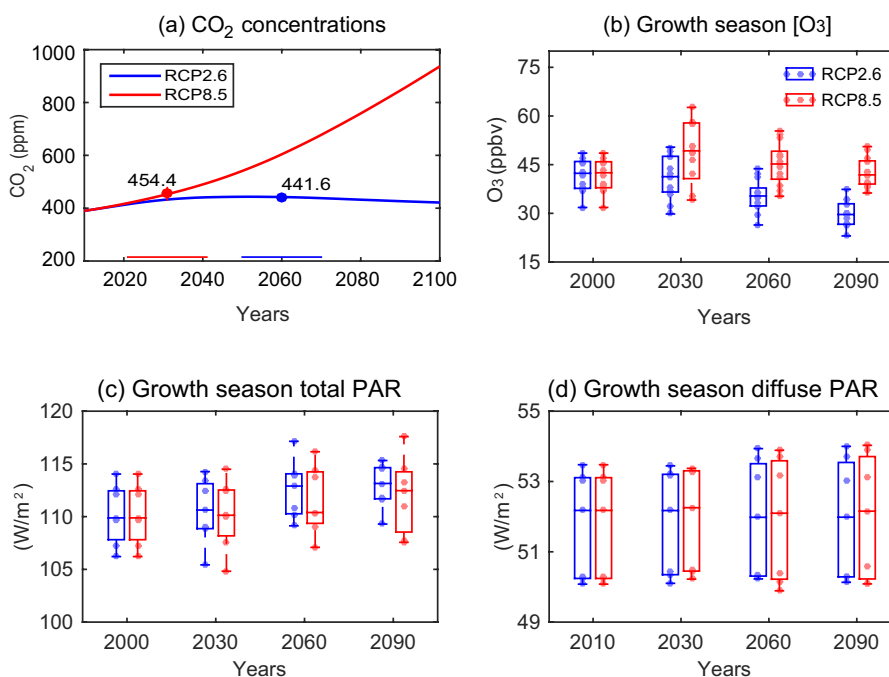
678

679



680

681



682

683

684 **Figure 3.** Changes in atmospheric compositions and radiation. Results shown are
685 projected future (a) global CO₂ concentrations, and (b) surface O₃ concentrations, (c)
686 total Photosynthetically Active Radiation (PAR), and (d) diffuse PAR at growth season
687 in China. The average (a) CO₂ concentrations at the global warming of 1.5°C are 442
688 ppm for RCP2.6 scenario (blue, 2050-2070) and 454 ppm for RCP8.5 scenario (red,
689 2021-2041). The (b) O₃ concentrations are averaged over east of 110°E in China from
690 12 ACCMIP models for RCP2.6 (blue) and RCP8.5 (red) scenarios. Each dot represents
691 the value averaged for May to September from a chemistry model. The (c-d) PAR
692 values are averaged over China from 7 CMIP5 models for RCP2.6 (blue) and RCP8.5
693 (red) scenarios. Diffuse PAR is calculated using hourly total PAR and solar zenith angle
694 based on the parameterization M01. Each dot represents the value averaged for May to
695 September from a climate model. For each selected year in (b-d), a period of 11 years
696 (5 years before and 5 years after) is used to derive the decadal mean values.

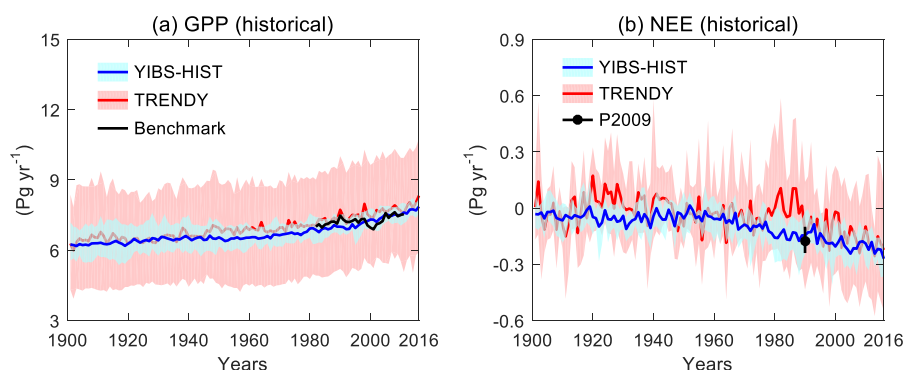
697

698

699



700
701



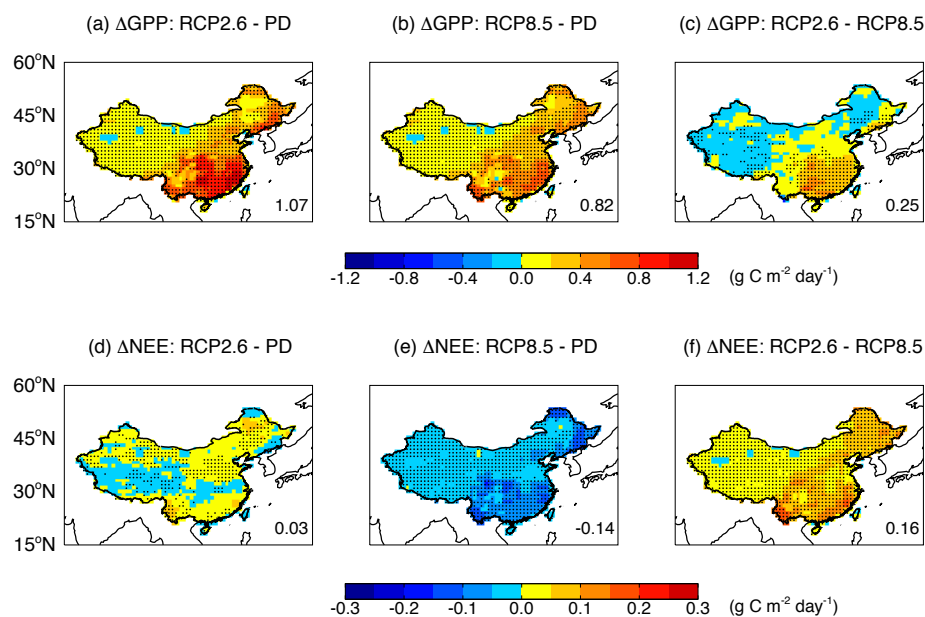
702
703
704
705
706
707
708
709
710
711
712
713
714
715

Figure 4. Historical carbon fluxes in China. Results shown are simulated (a) gross primary productivity (GPP) and (b) net ecosystem exchange (NEE) during historical period (1901-2016) using YIBs model (blue), and the comparison with predictions of 14 terrestrial models from TRENDY project (red). The bold lines are ensemble means with red shadings for inter-vegetation-model uncertainties and blue shadings for inter-climate-model uncertainties. All YIBs simulations are driven with daily meteorology from CMIP5 models. All TRENDY simulations are driven with CRUNCEP meteorology. The black line in (a) represents benchmark results of 1980-2011 from Jung et al. (2009). The black point with error bar in (b) represents the synthesis of ground- and model-based estimate of NEE in China by Piao et al. (2009).



716

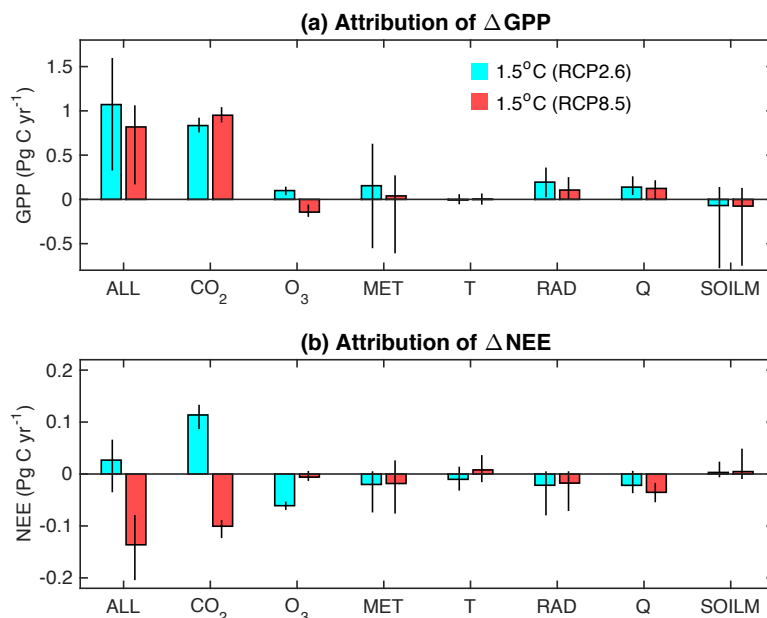
717



718

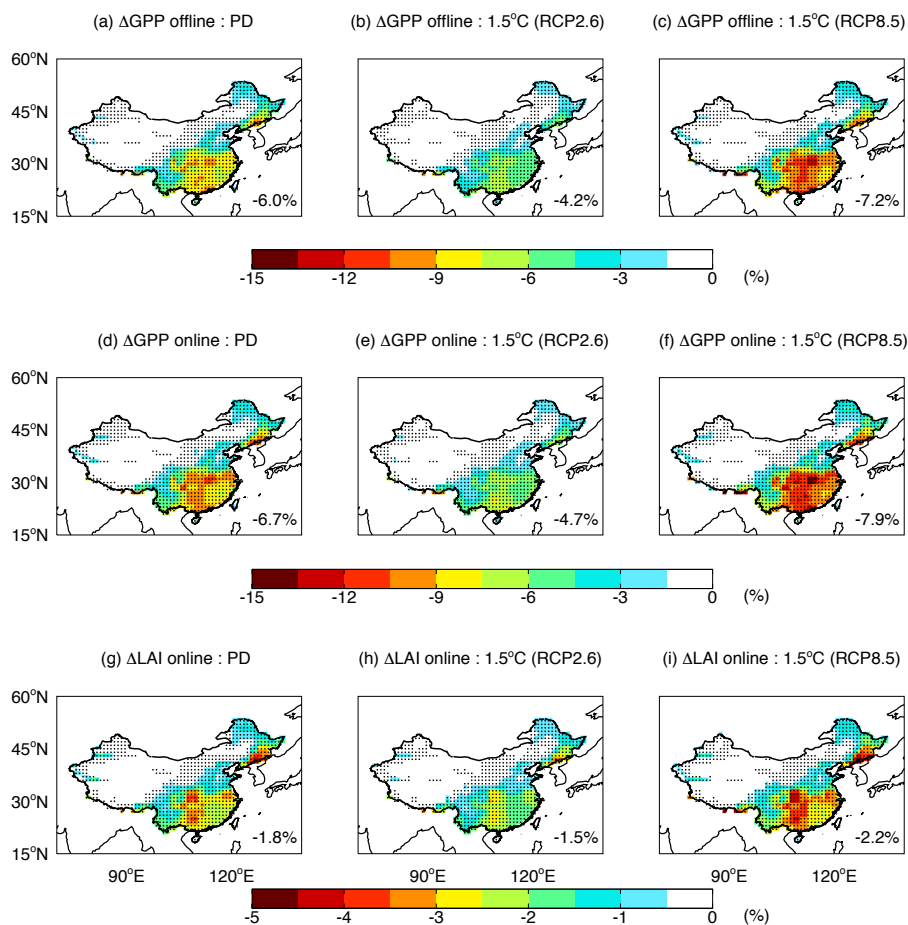
719 **Figure 5.** Changes in carbon fluxes by global warming of 1.5°C. Results shown are
720 simulated (top) GPP and (bottom) NEE over China between the period of global
721 warming of 1.5°C and present day (1995-2015) under (left) RCP2.6 scenario, (middle)
722 RCP8.5 scenario, and (right) their differences. The period of global warming of 1.5 °C
723 is set to 2050-2070 for RCP2.6 and 2021-2041 for RCP8.5. Simulations are performed
724 using YIBs vegetation model driven with daily meteorology from 7 CMIP5 models.
725 The O₃ damaging effect is included with predicted ensemble O₃ concentrations from 12
726 ACCMIP models. For each grid, significant changes at $p < 0.05$ are marked with dots.
727 The total changes (Pg C yr^{-1}) over China are shown in each panel.

728



729
730 **Figure 6.** Attribution of changes in GPP and NEE to individual driving factors. Results
731 shown are the predicted GPP changes in China between the period of global warming
732 of 1.5°C and present day (1995-2015) caused by all (ALL) or individual driving factors,
733 including CO₂ fertilization, O₃ damaging, and meteorological changes (MET). The
734 perturbations by meteorology is a combination of those by temperature (T), radiation
735 (RAD), specific humidity (Q), and soil moisture (SOILM). The contrast is shown
736 between the scenarios of RCP2.6 (blue, 2050-2070) and RCP8.5 (red, 2021-2041). The
737 error bars indicate uncertainties of YIBs simulations using different future meteorology
738 from 7 CMIP5 models.

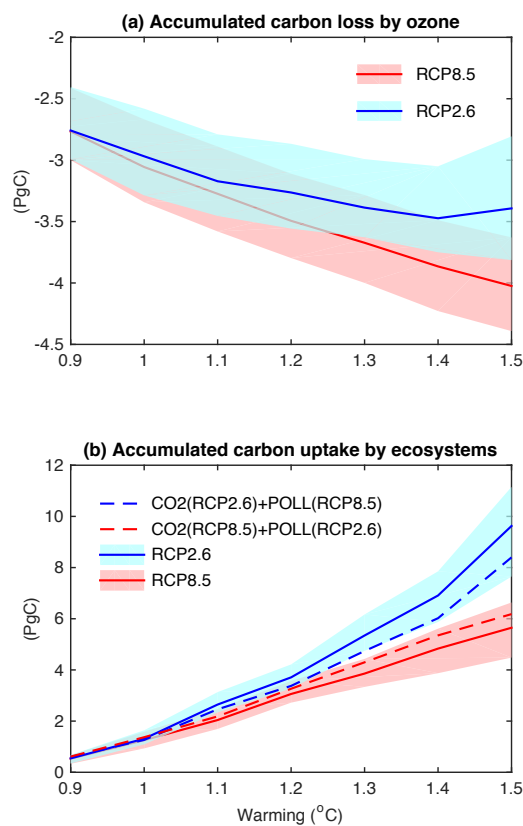
739
740
741



742
743 **Figure 7.** Damaging effects of O_3 to photosynthesis and plant growth. Results shown are ensemble
744 mean changes in (top) offline GPP, (middle) online GPP, and (bottom) leaf area index (LAI) caused
745 by O_3 at (left) present day (1995-2015) and 1.5°C warming under (middle) RCP.6 (2050-2070) and
746 (right) RCP8.5 (2021-2041) scenarios. The simulations are performed with YIBs vegetation model
747 driven with meteorology from 7 CMIP5 models and hourly ozone derived from 12 ACCMIP models.
748 The damaging effect is averaged for high and low O_3 sensitivities. For each grid, significant changes
749 at $p < 0.05$ are marked with dots. The mean changes over China are shown in each panel.
750



751



752

753 **Figure 8.** Accumulated carbon budget in China by 1.5°C global warming. The top panel
754 shows the total carbon loss of ecosystems caused by O₃ damaging effects at different
755 warming thresholds for two emission pathways. The bottom panel shows the total
756 carbon uptake by ecosystems in China at the 1.5°C global warming. The two solid lines
757 represent emissions of CO₂ and pollutants from the same scenario, either RCP2.6 (blue)
758 or RCP8.5 (red). The dashed lines represent sensitivity experiments with inconsistent
759 CO₂ and pollutants, with the blue (red) line driven with CO₂ from RCP2.6 (RCP8.5)
760 but air pollution from RCP8.5 (RCP2.6). The warming of 1.0 °C is the year 2010 for
761 both RCP2.6 and RCP8.5 scenarios.

762

763